# XMM-Newton-discovered Fast X-ray Transients: host galaxies and limits on contemporaneous detections of optical counterparts

Monthly Notices of the ROYAL ASTRONOMICAL SOCIETY

MNRAS **527,** 11823–11839 (2024) https://doi.org/10.1093/mnras/stad3924
Advance Access publication 2023 December 21

# XMM-*Newton*-discovered Fast X-ray Transients: host galaxies and limits on contemporaneous detections of optical counterparts

D. Eappachen [1,2]★ P. G. Jonker [1,2] J. Quirola-Vásquez [3,4,5] D. Mata Sánchez [6,7] A. Inkenhaag [2,1] A. J. Levan,[2] M. Fraser [8] M. A. P. Torres [6,7] F. E. Bauer,[3,4,9] A. A. Chrimes [2] D. Stern [10] M. J. Graham [11] S. J. Smartt [12] K. W. Smith,[12] M. E. Ravasio [2] A. I. Zabludoff [13] M. Yue [13,14] F. Stoppa [2,15] D. B. Malesani [16,17] N. C. Stone [18] and S. Wen [2]

*Affiliations are listed at the end of the paper*

Accepted 2023 December 19. Received 2023 December 14; in original form 2023 March 17

## ABSTRACT

Extragalactic fast X-ray transients (FXTs) are a class of soft (0.3–10 keV) X-ray transients lasting a few hundred seconds to several hours. Several progenitor mechanisms have been suggested to produce FXTs, including supernova shock breakouts, binary neutron star mergers, or tidal disruptions involving an intermediate-mass black hole and a white dwarf. We present detailed host studies, including spectroscopic observations of the host galaxies of seven *XMM-Newton*-discovered FXTs. The candidate hosts lie at redshifts $0.0928 < z < 0.645$ implying peak X-ray luminosities of $10^{43}$ erg s$^{-1}$ $< L_X < 10^{45}$ erg s$^{-1}$ and physical offsets of 1 kpc $< r_{\rm proj} <$ 22 kpc. These observations increase the number of FXTs with a spectroscopic redshift measurement by a factor of 2, although we note that one event is re-identified as a Galactic flare star. We infer host star formation rates and stellar masses by fitting the combined spectroscopic and archival photometric data. We also report on a contemporaneous optical counterpart search to the FXTs in *Pan-STARRS* and ATLAS by performing forced photometry at the position of the FXTs. We do not find any counterpart in our search. Given our constraints, including peak X-ray luminosities, optical limits, and host properties, we find that XRT 110 621 is consistent with an supernova shock breakout (SN SBO) event. Spectroscopic redshifts of likely host galaxies for four events imply peak X-ray luminosities that are too high to be consistent with SN SBOs, but we are unable to discard either the binary neutron star or white dwarf–intermediate-mass black hole tidal disruption event scenarios for these FXTs.

**Key words:** gamma-ray burst: general – X-rays: bursts – X-rays: general – supernovae: general – galaxies: general.

## 1 INTRODUCTION

Fast X-ray Transients (FXTs) are singular bursts of soft X-rays that last from minutes to hours, whose origin is still unknown. The majority (22 out of the 36) of the known FXTs have been discovered in *Chandra* archival data (see Jonker et al. 2013; Glennie et al. 2015; Irwin et al. 2016; Bauer et al. 2017; Xue et al. 2019; Lin, Irwin & Berger 2021; Quirola-Vásquez et al. 2022; Lin et al. 2022; Eappachen et al. 2023; Quirola-Vásquez et al. 2023), while 12 have been found in archival *XMM-Newton* data (Alp & Larsson 2020).[1] In addition, one FXT was discovered in eROSITA data (Wilms et al. 2020) and one in *Swift*/XRT data (XRT 080109/SN2008D; Soderberg et al. 2008). Earlier observatories are presumed to have detected some FXTs, but lacked sufficient spatial resolution to pinpoint them as extragalactic phenomena.

Among the 12 *XMM-Newton*-discovered FXTs, nine have candidate host galaxies, while for three no host has been identified to date. Alp & Larsson (2020) estimate the redshifts of those host galaxies to be between 0.1 and 1. Based on relatively limited photometric and spectroscopic information, they suggest that most of these FXTs are due to a supernova shock breakout (SN SBO). Specifically, these SN SBOs are consistent with the expectations for blue supergiant core-collapse supernovae (CC-SNe).

An SBO is predicted to be the first electromagnetic emission from a supernova explosion (Waxman & Katz 2017). This happens when the radiation-mediated shock crosses the surface of the star, thereby producing a bright X-ray/ ultraviolet (UV) flash on a timescale of seconds to a fraction of an hour (Falk & Arnett 1977; Klein & Chevalier 1978; Matzner & McKee 1999; Schawinski et al. 2008; Ganot et al. 2016; Waxman & Katz 2017). This is followed by months-long SN emission, which is predominantly powered by radioactive decay and detectable at UV/optical/near-infrared (IR) wavelengths. The SBO emission carries information about the progenitor star, potentially enabling the inference of physical properties of the progenitor such as the stellar radius and mass-loss history. If the circumstellar medium (CSM) is dense enough, the

★ E-mail: d.eappachen@sron.nl

[1] Note that out of the 12 *XMM-Newton*-discovered FXTs, three are suspected to be due to flares by late-type stars (Alp & Larsson 2020).

breakout will occur at larger radii within the CSM, resulting in a longer-duration transient event.

The only confirmed SN SBO observed to date is XRT 080109, associated with SN 2008D, serendipitously discovered in *Swift* observations of SN 2007uy (Soderberg et al. 2008). XRT 080 109 was detected in one of the arms of the spiral galaxy NGC 2770 at a distance of 27 Mpc. The X-ray light curve is characterised by a fast rise followed by an exponential decay with a peak X-ray luminosity of $\sim 6 \times 10^{43}$ erg s$^{-1}$. Based on the multiwavelength data set, Soderberg et al. (2008) shows that the observed properties are consistent with those of Wolf–Rayet stars ($R_* \sim 10^{11}$ cm), the favoured progenitors for type Ibc supernovae. More luminous SBOs have also been posited as an origin for some of the low luminosity long duration gamma-ray bursts (LGRBs) seen in the local Universe (e.g. GRB 060218; Campana et al. 2006).

Several other physical mechanisms have been suggested as the origin of FXTs; specifically a white dwarf (WD)–intermediate-mass black hole (IMBH) tidal disruption event (TDE) and a binary neutron star (BNS) merger. In general, the X-ray light curves of TDEs involving a main sequence star and a supermassive black hole have a time-scale ranging from months to years (Saxton et al. 2020). Instead, the relatively low mass of an IMBH compared to that of a supermassive black hole and the compactness of a WD compared to that of a main-sequence star implies that the time-scale associated with the X-ray light curve of IMBH-WD TDEs is much shorter than that of an SMBH – main-sequence TDE (Rosswog, Ramirez-Ruiz & Hix 2009; Maguire et al. 2020). A WD TDE remains a viable interpretation of at least some FXTs detected so far (e.g. XRT 000519; Jonker et al. 2013). In order to be consistent with the observed volumetric rates of FXTs (as reported by Quirola-Vásquez et al. 2023), one needs to assume that those IMBH-WD TDEs producing the X-ray emission are capable of launching jetted outflows. A beamed TDE emission would also naturally account for fairly high X-ray luminosities (MacLeod et al. 2016), similar to the ones observed in some FXTs. Indeed, there are also apparent similarities between these events and the sub-set of ultra-long duration gamma-ray bursts (Levan et al. 2014).

A BNS merger is another possible progenitor for FXTs. Some BNS mergers could leave behind supramassive or even stable magnetars, which are expected to produce FXTs (Dai et al. 2006; Metzger, Quataert & Thompson 2008; Zhang 2013; Metzger & Piro 2014; Sun, Zhang & Gao 2017). For some FXTs like CDF-S XT2 (Xue et al. 2019) and XRT 210 423 (Eappachen et al. 2023), the X-ray light curve shows a plateau and decay, similar to those seen in short gamma-ray bursts (SGRBs). This has been used as an argument in favour of a BNS origin. Since GW170817 it is known that SGRBs are caused by BNS mergers (Cowperthwaite et al. 2017). Converting the observed SGRB rate to an intrinsic rate that can be compared with the (nearly isotropic) FXT rate, a large beaming correction factor is required to reconcile the current observed FXTs volumetric density rate with that of SGRBs, providing potentially strong constraints on the opening angle of SGRB jets (Quirola-Vásquez et al. 2023).

While transient counterparts have been hard to find for FXTs (Bauer et al. 2017), we still expect progenitors of FXTs to be associated with a host. Host studies provide vital information to decipher the origin of the FXTs. For instance, finding the distance to the host galaxy helps constrain the energetics of the FXT (e.g. Eappachen et al. 2022, 2023). Understanding host environments can also play an important role in constraining the progenitor mechanism.

Host studies have been undertaken for a few of the *Chandra* FXTs. Bauer et al. (2017) finds a dwarf galaxy host ($m_r = 27.5$) at $\sim z_{\rm phot} = 0.4$–$3.2$ that lies 0.13 arcsec offset from the center of the X-ray uncertainty position of CDF-S XT1. Xue et al. (2019) reports that CDF-XT2 (Xue et al. 2019) lies at a projected distance of $3.3 \pm 1.9$ kpc from a $z_{\rm spec} = 0.74$ star-forming galaxy. Deep *Very Large Telescope* and *Gran Telescopio Canarias* (*GTC*) observations of XRT 000519 (Jonker et al. 2013) reveal a candidate host galaxy to the northwest of the FXT position in the $g$-band image at $m_g = 26.29 \pm 0.09$ mag (Eappachen et al. 2022) which, if the host galaxy – FXT association is real, rules out an SN SBO origin for this FXT. For XRT 170901, an elongated, possibly late-type, star-forming galaxy is reported by Lin et al. (2022) to fall within the $2\sigma$ X-ray position. No clear host galaxy was found for XRT 030 511 (Lin et al. 2022). For XRT 210423, Eappachen et al. (2023) report a candidate host that lies within the $3\sigma$ uncertainty region with a magnitude of $25.9 \pm 0.1$ in the *GTC*/HiPERCAM $g_s$-filter. In addition, they reported two other candidate host galaxies; one with $z_{\rm spec} = 1.5082 \pm 0.0001$ and offset $4.2 \pm 1$ arcsec ($37 \pm 9$ kpc) from the FXT position and another one with $z_{\rm phot} = 1.04^{+0.22}_{-0.14}$, offset by $3.6 \pm 1$ arcsec ($30 \pm 8$ kpc). Irrespective of which of these three candidate host galaxies is the real host galaxy, if one of them is the host, the properties are consistent with a BNS merger origin for XRT 210 423 (Eappachen et al. 2023).

In this paper, we look in detail at the host properties of seven of the *XMM-Newton*-discovered FXTs reported by Alp & Larsson (2020), namely XRT 161028, XRT 140811, XRT 030206, XRT 151219, XRT 151128, XRT 160220, and XRT 110621. We also search for contemporaneous optical counterparts for those FXTs where such observations exist in either *Pan-STARRS* (Chambers et al. 2016), DECam (Dark Energy Survey Collaboration 2016), or ATLAS (Tonry et al. 2018).

Throughout the paper, we assume a flat ΛCDM cosmology, with Hubble constant $\rm H_0 = 67.4 \pm 0.5\ km\,s^{-1}Mpc^{-1}$ and matter density parameter $\Omega_{\rm m} = 0.315 \pm 0.007$ (Planck Collaboration 2018). Throughout, magnitudes are quoted in the AB system. We use the term 'optical counterpart' for optical transient light associated with the FXT, and 'candidate host' or 'candidate host galaxy' for the host galaxy of the FXT. The uncertainties mentioned in the paper are at the $1\sigma$ confidence level, unless mentioned otherwise.

## 2 OBSERVATIONS AND ANALYSIS

In order to determine the redshift of the candidate host galaxy, and thus distance to the FXT and the host properties, we obtained spectroscopic observations of candidate host galaxies to a subset of the FXTs reported in Alp & Larsson (2020). A journal of the spectroscopic observations is given in Table 1.

### 2.1 Astrometry

We reviewed the FXTs reported by Alp & Larsson (2020) in the *XMM-Newton* serendipitous catalogue (Webb et al. 2020). We have updated the Right Ascension (RA) and Declination (Dec.) and the associated uncertainty region for the FXTs discussed in the paper, see Table 2. In the *XMM-Newton* serendipitous catalogue X-ray detection astrometry is improved by cross-correlating X-ray detections with optical or infrared catalogues like USNO B1.0, 2MASS, or SDSS (DR8). For the FXT, XRT 110621 we use the coordinates and X-ray uncertainty reported by Novara et al. (2020) in which they cross-match the brightest sources detected in the XMM–Newton observation with the USNO B1 optical catalogue (Monet et al. 2003).

**Table 1.** A journal of the spectroscopic observations of the candidate host of the *XMM-Newton*-discovered FXTs used in this paper.

| Target | Telescope/Instrument | Date (UT) | Observations | Grism | Exposure time [s] | Airmass | Seeing (arscec) |
|---|---|---|---|---|---|---|---|
| XRT 161028 | *GTC*/OSIRIS | 2022 September 19 | 3 | R500R | 600 | 1.1 | ∼0.7 |
| XRT 140811 | *GTC*/OSIRIS | 2022 September 19 | 3 | R500R | 600 | 1.3 | ∼0.8 |
| XRT 030206 | *GTC*/OSIRIS | 2022 September 19 | 1 | R500R | 2650 | 1.3 | ∼0.9 |
| XRT 151219 | *Keck*/LRIS | 2022 November 25 | 2 | Blue/600 and Red/400 | 1200 | 1.4 | ∼0.9 |
| XRT 151128 | *Keck*/LRIS | 2022 November 25 | 2 | Blue/600 and Red/400 | 1200 | 1.3 | ∼1.0 |
| XRT 160220 | *Magellan*/LDSS3 | 2021 August 02 | 3 | VPH-All | 900 | 1.3 | ∼1.2 |
| XRT 110621 | *Magellan*/LDSS3 | 2021 August 02 | 3 | VPH-All | 900 | 1.2 | ∼1.2 |

**Table 2.** The updated the RA and Dec. and the associated X-ray uncertainty region of the FXTs obtained from the *XMM-Newton* serendipitous catalogue.

| FXT | RA J2000 (°) | Dec. J2000 (°) | X-ray uncertainty ($1\sigma$) (arcsec) |
|---|---|---|---|
| XRT 161028 | 263.23645 | 43.51225 | 1.1 |
| XRT 140811 | 43.65351 | 41.07393 | 1 |
| XRT 030206 | 29.28802 | 37.62769 | 0.8 |
| XRT 151219 | 173.53129 | 0.87324 | 1.3 |
| XRT 151128 | 167.07858 | −5.07474 | 1.8 |
| XRT 160220 | 204.19900 | −41.33699 | 1.6 |
| *XRT 110621 | 37.89542 | −60.62869 | 1.9 |

* From Novara et al. (2020).

### 2.2 Optical spectroscopic observations

#### *2.2.1* GTC *OSIRIS*

We obtained spectra of candidate host galaxies for the FXTs XRT 161028, XRT 140 811, and XRT 030 206 using the Optical System for Imaging and low-Intermediate-Resolution Integrated Spectroscopy (OSIRIS; Cepa et al. 2000) instrument mounted on the 10.4-m *GTC*. We used the R500R grism and 1 arcsec-wide slit (4800–10000 Å with a moderate resolving power of R ≈ 350 at $\lambda_c$ = 7165 Å). The spectrum was recorded on a mosaic of two Marconi CCDs. We undertook bias subtraction, flat field correction, and spectral extraction using PYRAF (Science Software Branch at STScI 2012) and wavelength (arc lamps Xe, Ne and HgAr) and flux calibration using MOLLY (Marsh 2019).

#### *2.2.2* Keck *LRIS*

We observed XRT 151219 and XRT 151128 on UT 2022 November 25 using the Low-Resolution Imaging Spectrometer (LRIS; Oke et al. 1995) on the *Keck* I telescope. For both sources, we obtained two 1200 s exposures using the 600 $\ell$ mm$^{-1}$ blue grism ($\lambda_{\rm blaze}$ = 4000 Å), the 400 $\ell$ mm$^{-1}$ red grating ($\lambda_{\rm blaze}$ = 8500 Å), the 5600 Å dichroic, and the 1-arcsec slit. This instrument configuration covers the full optical window at moderate resolving power, $R \equiv \lambda/\Delta\lambda \approx 1500$ for objects filling the slit. Because this was a half-night allocation with only a single standard observation, we used archival observations of standard stars from Massey & Gronwall (1990) observed in 2020 January with the same instrument configuration for flux calibration. We reduced the spectra using standard techniques with IRAF (Tody 1986).

#### *2.2.3 Magellan LDSS3*

The Low Dispersion Survey Spectrograph (LDSS-3) is a spectrograph mounted on the 6.5-m *Magellan* telescope at the Las Campanas Observatory in Chile. We obtained spectra of the host candidates for XRT 160 220 and XRT 110 621 using LDSS-3. We used the VPH-All grism and a 1-arcsec slit width (covering 4250–10000 Å with a resolving power of R ≈ 1150 at $\lambda_c$ = 7100 Å) for our observations. We used PYRAF scripts (Science Software Branch at STScI 2012) for cleaning and reducing the data and MOLLY (Marsh 2019) for wavelength (using the He, Ne, and Ar arc lamps) and flux calibration.

### 2.3 Optical photometric observations

In addition to our targeted observations to obtain galaxy redshifts, we also make use of archival imaging surveys to provide photometric measurements of the host galaxies, and for surveys where the temporal coverage matches the FXT event, we extract forced photometry around the time of the FXT detection. Optical photometry of seven candidate host galaxies is given in Table 3.

#### *2.3.1* Pan-STARRS *and Blanco/DECam*

The *Panoramic Survey Telescope and Rapid Response System* (*Pan-STARRS*; Chambers et al. 2016) is a 1.8-m telescope located at Haleakala Observatory, Hawaii. It uses a 1.4 Gigapixel camera to image the sky in five broad-band filters ($g$, $r$, $i$, $z$, $y$). *Pan-STARRS* operations began on 2010 May 13. We obtained deep stacked *Pan-STARRS* images of the fields of the FXTs. Deep *Pan-STARRS* or Dark Energy Camera (DECam) images of the field of the seven FXTs under study here are shown in Fig. 1. For each FXT, we show the filter image where the host candidate is most clearly visible. Red circles show the $1\sigma$ confidence error region of the FXT. The candidate host galaxies are marked with yellow lines. We used SEXTRACTOR (Bertin & Arnouts 1996) to extract the RA and Dec. from the centre of the candidate host galaxies using the *Pan-STARRS* images. The positions of the host galaxies are then used to calculate the angular and physical offset between the centre of the candidate host galaxy and the centre of the FXT X-ray location for each FXT. We also performed forced photometry at the position of the FXTs in *Pan-STARRS* (Magnier et al. 2020). We use the point spread function derived from the image to determine the upper limit on the photometry at the known, fixed,

**Table 3.** Host photometry and position of the candidate FXT host galaxies.

| Host galaxy of | RA and Dec. J2000 (°) | Source | $m_u$ (AB mag) | $m_g$ (AB mag) | $m_r$ (AB mag) | $m_i$ (AB mag) | $m_z$ (AB mag) | $m_y$ (AB mag) |
|---|---|---|---|---|---|---|---|---|
| XRT 161028 | 263.23707–43.51231 | SDSS17/*Pan-STARRS* | $22.3 \pm 0.3$ | $21.19 \pm 0.06$ | $20.83 \pm 0.04$ | $20.64 \pm 0.04$ | $20.57 \pm 0.06$ | – |
| XRT 140811 | 43.65365–41.07406 | *Pan-STARRS* | – | $21.80 \pm 0.06$ | $20.61 \pm 0.02$ | $19.71 \pm 0.01$ | $19.32 \pm 0.02$ | $19.02 \pm 0.04$ |
| XRT 030206 | 29.28776–37.62768 | *Pan-STARRS* | – | $21.89 \pm 0.11$ | $22.05 \pm 0.12$ | $22.37 \pm 0.11$ | $21.73 \pm 0.15$ | – |
| *XRT 151219 | 173.53037 0.87409 | SDSS17/PS/VIKING | $22.2 \pm 0.4$ | $22.4 \pm 0.2$ | $21.6 \pm 0.1$ | $21.05 \pm 0.05$ | $20.82 \pm 0.06$ | $20.4 \pm 0.2$ |
| XRT 151128 | 167.07885–5.07495 | *Pan-STARRS* | – | $21.5 \pm 0.1$ | $20.30 \pm 0.04$ | $19.83 \pm 0.03$ | $19.47 \pm 0.03$ | $19.63 \pm 0.09$ |
| **XRT 160220 | 204.19926–41.33718 | DECam/VHS | – | – | – | $22.25 \pm 0.05$ | $21.23 \pm 0.04$ | – |
| ***XRT 110621 | 37.89582–60.62918 | GROND | – | $19.58 \pm 0.01$ | $19.58 \pm 0.01$ | $19.53 \pm 0.01$ | $19.67 \pm 0.02$ | – |

*(AB mag) $m_J = 20.5 \pm 0.2$, $m_H = 20.2 \pm 0.3$, $m_K = 19.9 \pm 0.2$

**(AB mag) $m_J = 20.25 \pm 0.28$ ***(AB mag)$m_J = 19.39 \pm 0.07$, $m_H = 19.63 \pm 0.14$, $m_K = 19.67 \pm 0.18$; From Novara et al. (2020)

FXT position in the difference images. The $5\sigma$ limiting magnitudes of stacked *Pan-STARRS* images in the $g$, $r$, $i$, $z$, and $y$ filters are 23.3, 23.2, 23.1, 22.3, and 21.4 mag, respectively (Chambers et al. 2016).

We used deep images of the field of the FXTs XRT 160220 and XRT 110621 obtained using the DECam, mounted on the *Blanco* 4-m Telescope at Cerro Tololo Inter-American Observatory (Dark Energy Survey Collaboration 2016). The DECam fields of XRT 160220 and XRT 110621 are shown in Fig. 1. The $10\sigma$ limiting magnitude for galaxies in Dark Energy Survey utilizing DECam is $g = 23.4$, $r = 23.2$, $i = 22.5$, $z = 21.8$, and $Y = 20.1$ (Drlica-Wagner et al. 2018).

#### 2.3.2 *ATLAS*

The Asteroid Terrestrial-impact Last Alert System (ATLAS) is a robotic astronomical survey (Tonry et al. 2018) which maintains a quadruple 0.5 m telescope system with two units in Hawaii and one each in Chile (El Sauce) and South Africa (Sutherland). ATLAS observes the whole visible sky several times every night to a limiting magnitude in the *o*-filter (5600–8200 Å) of $\sim 19.5$. We also obtained upper limits to the flux density at the position of FXTs using the ATLAS forced photometry server (Smith et al. 2020).

#### 2.3.3 *ESO–2.2m/GROND*

The Gamma-ray Burst Optical/Near-infrared Detector (GROND; Greiner et al. 2008) is attached to the *MPG/ESO* 2.2-m telescope located at the La Silla Observatory. We adopt the GROND photometric data for XRT 110621 reported by Novara et al. (2020).

#### 2.3.4 *SDSS*

The Sloan Digital Sky Survey (SDSS) uses a 2.5-m optical telescope dedicated to a multispectral imaging and a spectroscopic redshift survey. We use the SDSS17 (Abdurro'uf et al. 2022) photometric data for some of the candidate hosts.

### 2.4 Near-infrared photometric observations

#### 2.4.1 *VISTA*

The *Visible and Infrared Survey Telescope for Astronomy* (*VISTA*; Dalton et al. 2006), part of ESO's Paranal Observatory, is a 4-m-class telescope. VIKING is the *VISTA* Kilo-Degree Infrared Galaxy Survey (Edge et al. 2013). We use photometric data from VIKING for XRT 151219. The *VISTA* Hemisphere Survey (VHS; McMahon et al. 2013) is imaging the entire southern hemisphere of the sky in at least two infrared filters ($J$ and $K_s$). We obtain the $J$-filter magnitude for XRT 160220 from VHS.

## 3 RESULTS

### 3.1 Forced photometry

We performed forced photometry using *Pan-STARRS*, and the ATLAS forced photometry servers for FXTs XRT 161028, XRT 151219, XRT 151128, and XRT 160220. Fig. 2 shows the resulting light curves, with time in Modified Julian Date (MJD) and 1-d average fluxes and uncertainties (in $\mu$Jy) from 30 d before to 200 d after the date of occurrence of the FXT (indicated by the grey vertical dashed line). No contemporaneous counterpart ($5\sigma$ detection threshold) was found for any of these FXTs. Different filters are indicated with different colours. For XRT 140811, XRT 030206, and XRT 110621, no forced photometry results are available within 200 d of the event.

We derive upper limits by converting the flux density measurement uncertainty to an AB magnitude (we take $5\times$ the uncertainty in the flux density measurement for the upper limit calculation). The AB magnitude upper limit inferred from the forced photometry is given in Table 4. The observation closest in time to the FXT is that in the $z$-filter for XRT 161028 in *Pan-STARRS*. It is $\sim$170 d after the burst. In the case of XRT 151219, there are multiband observations of the field of the FXT $\sim$25 d after the transient. We also have *Pan-STARRS* observations within $\sim$25 d and ATLAS observations within a day after XRT 151128.

We use the statistical test ConTEST (Stoppa, Cator & Nelemans 2023), developed explicitly for astronomical data coupled with measurement uncertainties, to check for consistency between the observations and a constant model at zero. The null hypothesis of consistency is tested by calculating a distance measure, the test statistic $t$, between the observations and the model. This step is then followed by a simulation-based methodology where the model is assumed to be the ground truth, and a high number of samples are generated from it based on the observed uncertainties. Calculating the test statistic for each new simulated sample and comparing all of them to the test statistic of the original observations allows us to interpret whether the assumption of consistency has been violated or not. For an observed test statistic $t$ from an unknown distribution $T$, the P-value is the probability of observing a test-statistic value as extreme as the one observed if the null hypothesis $H_0$ were true. For a two-tailed test, that is,

$$P - value = 2 \times min\{P(t \geq T|H_0), P(t < T|H_0)\}.$$

The null hypothesis is not rejected when the P-value is greater than the significance level $\alpha$, which, in our case, is set to the standard value

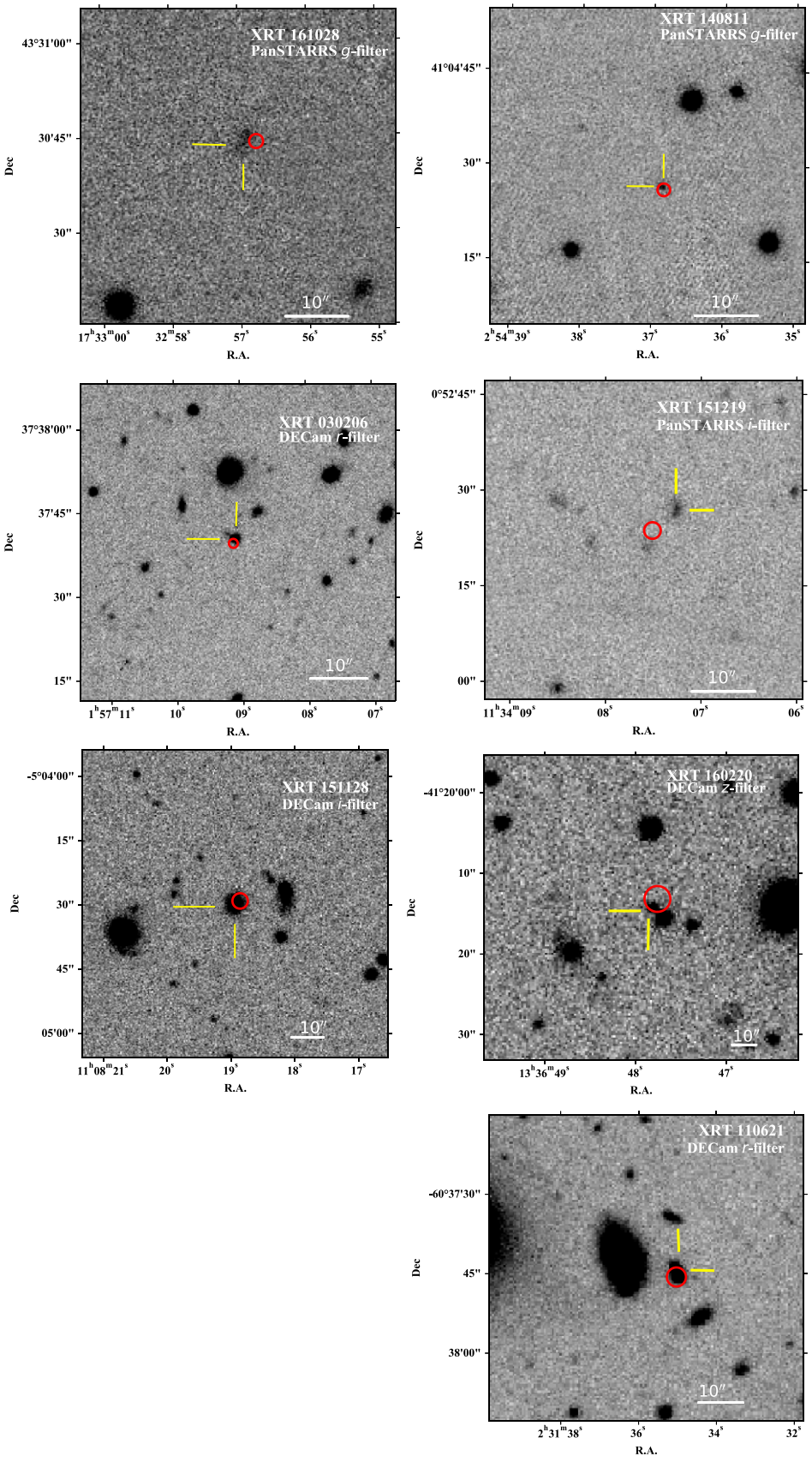


**Figure 1.** Deep stacked *Pan-STARRS* or DECam images of the field of seven of the twelve *XMM-Newton*-discovered FXTs reported by Alp & Larsson (2020). The red circles show the 1$\sigma$ X-ray positional uncertainty region of the FXT, while the candidate hosts are marked with yellow lines.

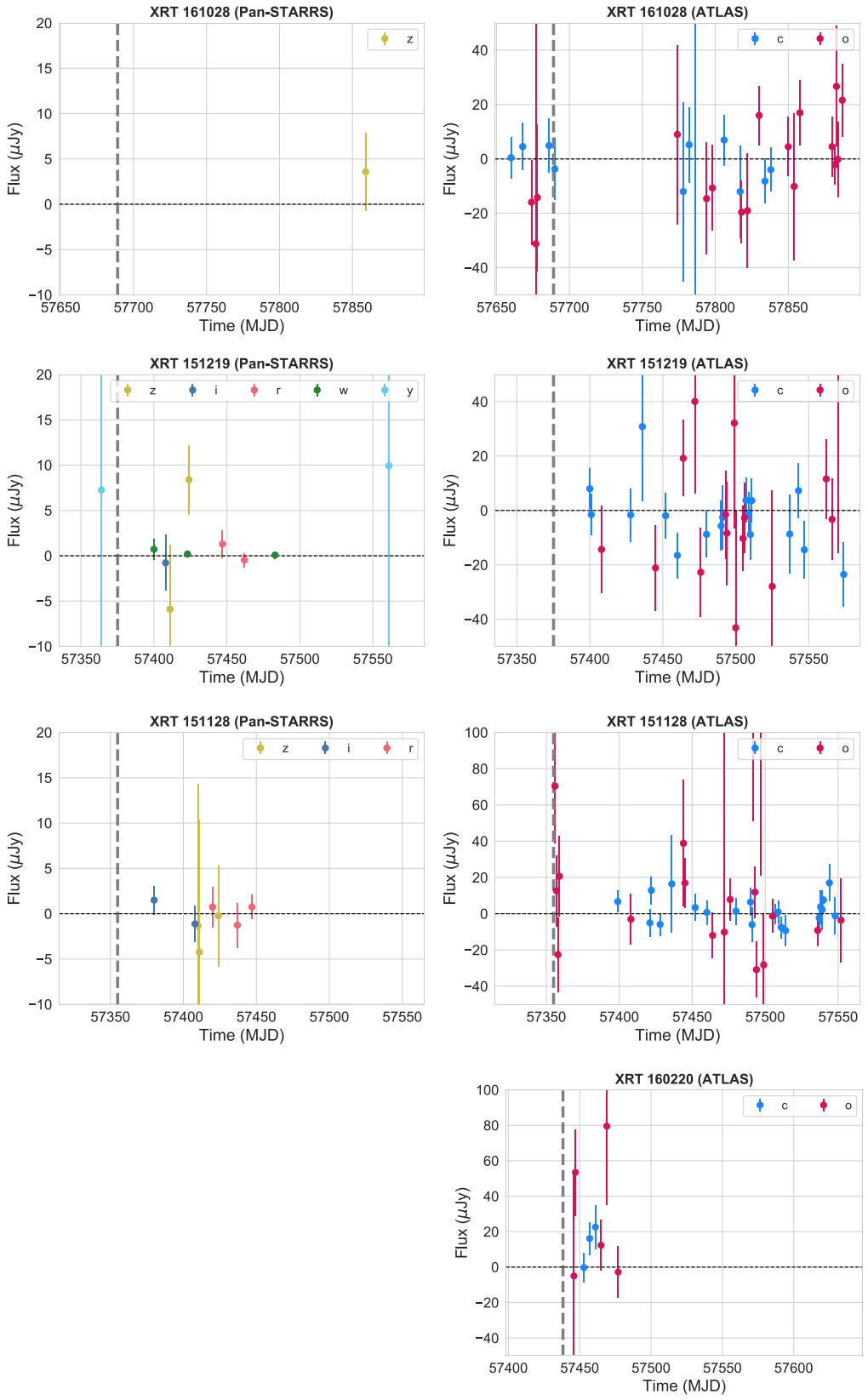


**Figure 2.** The results of the *Pan-STARRS* and ATLAS forced photometry starting 30 d before and lasting 200 d after the FXT for XRT 161028, XRT 151219, XRT 151128, and XRT 160220. The *x*-axis shows time in MJD, and the *y*-axis shows the 1-d average flux densities and their uncertainties (in $\mu$Jy). Different filters are indicated by different colours. The vertical dashed grey line indicates the time the FXT occurred. No optical source was detected to 5$\sigma$ limits at the FXT location in any filters for any of these FXTs.

**Table 4.** The $5\sigma$ upper limits (AB mag) inferred from forced photometry.

| FXT | Time (MJD) | Pan-STARRS filters | *Pan-STARRS* $5\sigma$ upper limits (AB mag) | $\sim\Delta T_{\rm PS}$ (d) | ATLAS filters | ATLAS $5\sigma$ upper limits (AB mag) | $\sim\Delta T_{\rm ATLAS}$ (d) |
|---|---|---|---|---|---|---|---|
| XRT 161028 | 57689.1108 | $z$ | 20.6 | 170 | $c$, $o$ | 19.5, 18.4 | 01, 85 |
| XRT 151219 | 57375.1343 | $w^{\star}$, $z$ | 22.0, 20.7 | 25, 49 | $c$ | 20.0 | 25 |
| XRT 151128 | 57354.9722 | $i$, $r$ | 21.7, 21.3 | 26, 66 | $o$ | 18.4 | 01 |
| XRT 160220 | 57438.3113 | – | – | – | $o$, $c$ | 18.7, 19.8 | 09, 15 |

$^{\star}$A wide filter denoted by $w$, that essentially spans the *gri* filters.

$\alpha = 0.05$. In ConTEST, the P-value is estimated as the proportion of test statistics of the simulated samples that have a $t$-value larger than that derived for the observation – model combination. As shown in Fig. 3, another way to evaluate the result of the test is checking that the test statistic $t$ lies between the two critical values, that, for a significance level $\alpha = 0.05$, are the 2.5 and 97.5 percentiles of the simulations' distances distribution. We performed this test considering different time periods of 0–100 and 0–200 d after the FXT onset in different filters. Due to the lack of data points in the forced photometry light curve, we only did this test in one setting (0–200 d) for the *Pan-STARRS* data, considering the data points from all the filters together.[2] For all the cases, the null hypothesis is not rejected; hence, the model of zero flux density detected in the period 0–200 d after the FXT is consistent with the observations. Fig. 3 shows an example of the output of the statistical test ConTEST performed on the ATLAS forced photometry data (using the $c$-filter data) of XRT 151219. We find that the forced photometry light curves for XRT 161028, XRT 151219, XRT 151128, and XRT 160220 show no evidence for the detection of an optical source with a flux density above our upper limits.

### 3.2 Identification, photometry, and spectroscopy of candidate host galaxies

For each of the FXTs listed below, we searched for a candidate host galaxy in either DECam or *Pan-STARRS* images. If a candidate host galaxy is found we determine its chance alignment probability in the following way: we determined the density of sources as bright as or brighter than the object in the filter under consideration in a square region, we provide the coordinate centres of this region, the size of the region, the measured source density, and the filter under consideration in Table 5. Assuming Poisson statistics and considering the area of the error region, we compute the probability of a chance alignment for each FXT (see Table 5).

#### *3.2.1 XRT 161028*

An extended object is found in *Pan-STARRS* images (*top left* panel of Fig. 1) at (RA, Dec.) = (263.°23707, 43.°51231). The centroid of this object is offset by $1.7 \pm 1.1$ arcsec from the X-ray position. The source has a kron magnitude of $r = 20.69 \pm 0.05$ and a $g$–$r$ colour of $0.36 \pm 0.07$.

The spectrum of the candidate host galaxy XRT 161028 (shown in the *top* panel of Fig. 5) exhibits the emission lines H $\alpha$ $\lambda$6564.6,[3] H $\beta$ $\lambda$4862.7, [O II] $\lambda$3728.5, [O III] $\lambda$4960.3, 5008.2, and absorption line Mg$\lambda$5176.7. We fitted multiple Gaussians to the emission and absorption line using the LMFIT[4] package and obtained the best-fitting central wavelengths and their associated errors. We determine that the redshift of the galaxy is $z_{\rm spec} = 0.326 \pm 0.004$.

In the *GTC*/OSIRIS spectroscopic acquisition image for the field of XRT 161028, the host candidate appears to be an extended object (see Fig. 4). However, upon the inspection of the spectroscopic data, we find that the source is a blend of two objects. We extracted both traces and found another candidate host at redshift $z_{\rm spec} = 0.645 \pm 0.007$. We identify the emission lines H $\beta$ $\lambda$4862.7, [O II] $\lambda$3728.5, [O III] $\lambda$5008.2, and the absorption line Mg $\lambda$5176.7. These candidate hosts both lie within the $3\sigma$ X-ray position.

#### *3.2.2 XRT 140811*

The spectrum of the host candidate of XRT 140811 is consistent with the spectrum of a K3-star. Fig. 6 shows the 5000–8500 Å *GTC*/OSIRIS spectrum of the candidate counterpart of XRT 140811 and K-star template spectrum from the ESO stellar library (Pickles 1998). Therefore, we do not consider this object any further.

#### *3.2.3 XRT 030206*

XRT 030206 is offset by $0.8 \pm 0.8$ arcsec from the centre of a candidate host galaxy at (RA, Dec.) = (29.°28776, 37.°62768) (*second row-left* panel of Fig. 1). The candidate host for XRT 030206 has $r = 22.05 \pm 0.12$.

The extracted 1D spectrum of the candidate host galaxy of XRT 030206 shows [O III] $\lambda$4960.3, 5008.2 and H $\alpha$ $\lambda$6564.6 emission lines. We also identify extended emission in the 2D spectrum of the candidate host at the position of [O III] and H $\alpha$. We infer the spectroscopic redshift of the candidate host of XRT 030206 to be $z_{\rm spec} = 0.281 \pm 0.003$. The residuals due to the subtraction of bright sky emission lines are present in the part of the spectrum we marked with a grey vertical band (*second* panel of Fig. 5). We visually inspected the 2D spectrum and determined that these are due to contamination from sky lines, particularly since there are no bright emission lines expected at these wavelengths (given the redshift derived from [O III] and H $\alpha$).

#### *3.2.4 XRT 151219*

In the *Pan-STARRS* $i$-filter image of XRT 151219 (*second row-right* panel in Fig. 1), two candidate host galaxies can be identified. We consider the extended galaxy at an offset of $4.9 \pm 1.3$ arcsec as the probable host (marked with yellow lines).

[2]This somewhat unrealistically tests for the presence of a source with an emission spectrum that is flat over the optical bands.

[3]Rest wavelengths of the lines in vacuum are from https://classic.sdss.org/dr6/algorithms/linestable.html

[4]https://lmfit.github.io/lmfit-py/

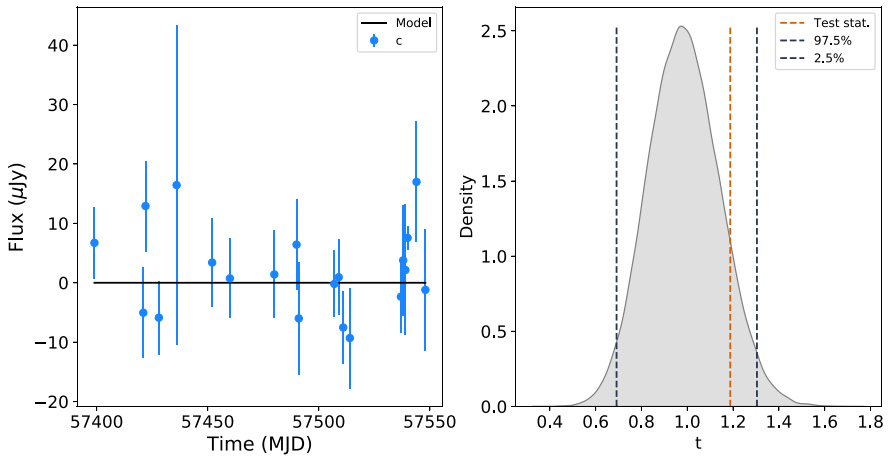


**Figure 3.** Results of the CONTEST (Stoppa, Cator & Nelemans 2023) test performed on the ATLAS forced photometry data (using the *c*-filter observations) of XRT 151219. *Left panel*: The flux density, relative uncertainties (blue dots and bars), and the constant at zero model (black line) are shown. *Right panel*: The test statistic (orange dashed line) is found to lie between the two critical values, that, for a significance level $\alpha = 0.05$, are the 2.5 and 97.5 percentiles of the simulations' distances distribution. We find that the null-hypothesis of consistency at zero is not rejected.

**Table 5.** Chance alignment probabilities.

| Candidate host of | Coordinate centres of the region used for density determination (RA and Dec. in °) | Filter | Region considered (arcsec) | Source density (#/arcsec$^{-2}$) | Radius of interest (arcsec) | Chance alignment probability (per cent) | Positional Uncertainty ($1\sigma$) (arcsec) |
|---|---|---|---|---|---|---|---|
| XRT 161028 | 263.°23650, 43.°51246 | *Pan-STARRS g* | 70 × 70 | 0.0008 | 1.7 | 0.7 | 1.1 |
| XRT 140811 | 43.°65379, 41.°07421 | *Pan-STARRS g* | 70 × 70 | 0.002 | 1 | 0.6 | 1 |
| XRT 030206 | 29.°287789037, 7.°6276687 | DECam *r* | 57 × 57 | 0.002 | 0.8 | 0.4 | 0.8 |
| XRT 151219 | 173.°53100, 0.°87342 | *Pan-STARRS i* | 70 × 70 | 0.0008 | 4.9 | 5.8 | 1.3 |
| XRT 151128 | 167.°07797, −5.°07520 | DECam *i* | 70 × 70 | 0.0008 | 1.8 | 0.8 | 1.8 |
| XRT 160220 | 204.°19986, −41.°33725 | DECam *z* | 38 × 38 | 0.007 | 1.6 | 5.2 | 1.6 |
| XRT 110621 | 37.°89449 −60.°62715 | DECam *r* | 70 × 70 | 0.0004 | 1.9 | 0.5 | 1.9 |

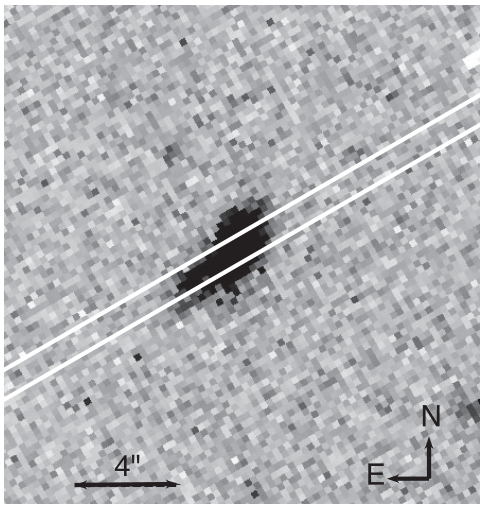


**Figure 4.** The *GTC*/OSIRIS the *r*-filter acquisition image of the candidate host of XRT 161028 (compare with the top left panel of Fig. 1). The 1-arcsec slit is placed at a position angle of 120° North through East. This extended object is a blend of two (extended) sources as is also evident from the spectroscopic data.

For the candidate host galaxy of XRT 151219, we determine the redshift using the emission lines H $\beta$ $\lambda$4862.7 and [O II] $\lambda$3728.5 to be $z_{\rm spec} = 0.584 \pm 0.009$. Other lines, such as [O III] $\lambda$4960.3, 5008.2, and Mg II$\lambda$2799.1, can be identified in the spectrum (*third* panel of Fig. 5) and they support this redshift determination.

### 3.2.5 XRT 151128

A possible host galaxy is detected in the DECam *i*-filter (*third row left* panel in Fig. 1) with an offset of $1.2 \pm 1.8$ arcsec. The photometry of XRT 151128 is given in Table 3.

The candidate host galaxy of XRT 151128 has a redshift of $z_{\rm spec} = 0.509 \pm 0.009$. The redshift was derived through fitting Gaussians to the emission line and the absorption lines [O III] $\lambda$5008.2, Mg$\lambda$5176.7 and Mg II$\lambda$2799.1. The flux calibrated spectrum of XRT 151128 is shown in the *fourth* panel of Fig. 5.

### 3.2.6 XRT 160220

The *z*-filter DECam image of the field of XRT 160220 is shown in the *third row-right* panel of Fig. 1. The DECam/VHS photometry of the host of XRT 160220 is given in Table 3. This host galaxy was identified within the $1\sigma$ X-ray position by Alp & Larsson (2020), marked by the yellow pointers in Fig. 1. The spectrum is dominated

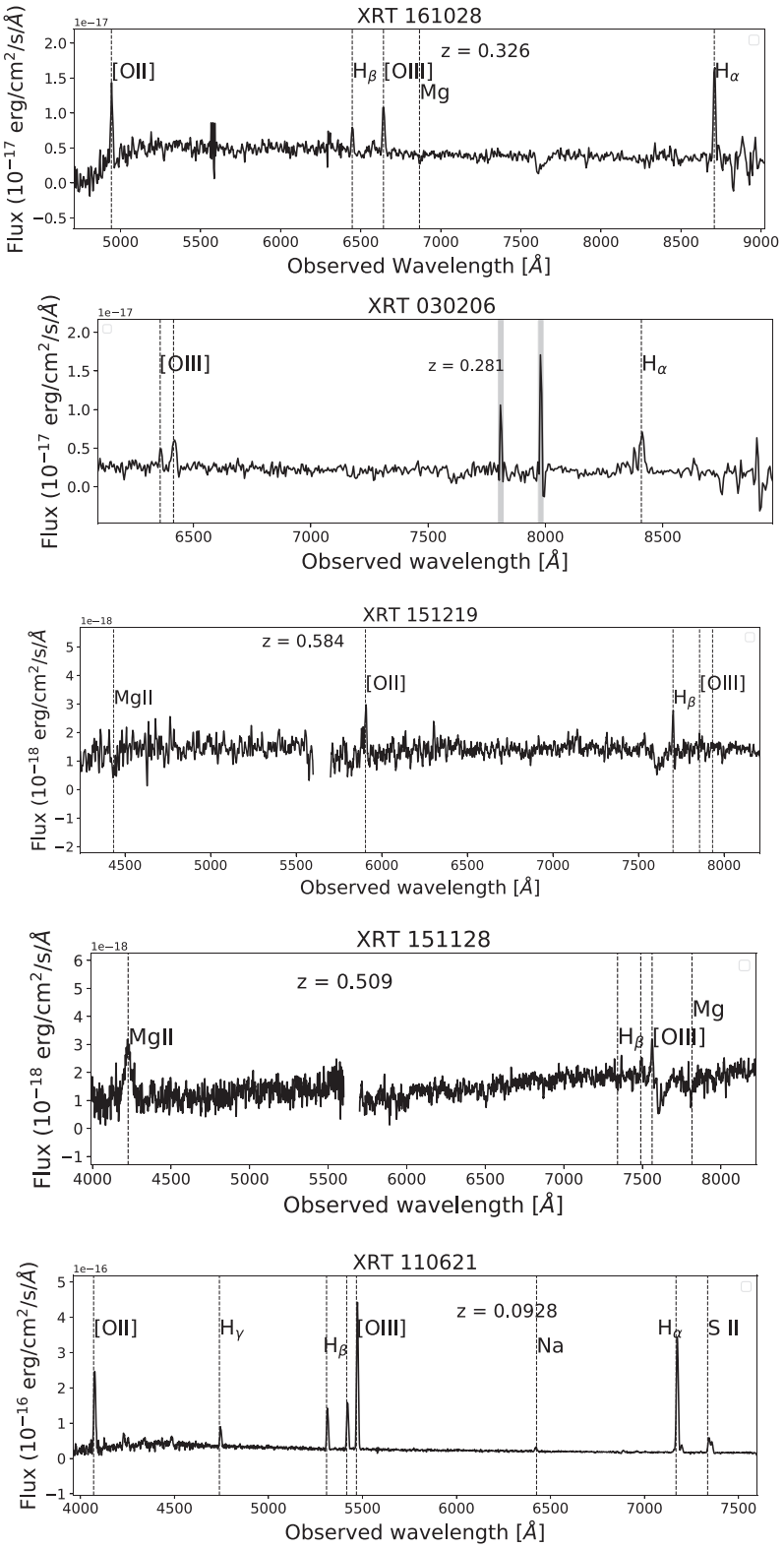


**Figure 5.** The flux-calibrated spectra of five of the seven candidate hosts galaxies shown in Fig. 1. For display purposes the boxcar smoothed spectrum (Box1DKernel with a width of 3 pixels) is shown for XRT 151219 and XRT 151128. Dashed vertical lines mark the location of important emission and absorption lines in each of the spectra. For XRT 030206, there are sky residuals present in the spectrum towards the redder part of the spectrum (marked in grey).

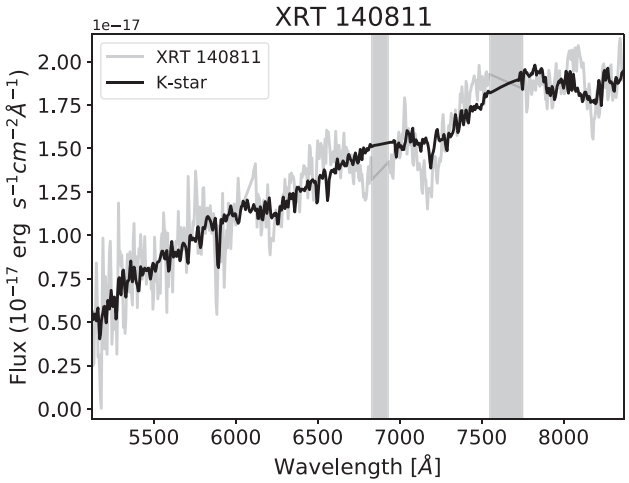


**Figure 6.** The *GTC*/OSIRIS spectrum of the candidate host of XRT 140811 in the wavelength range 5000–8500 Å. A K3V-star template spectrum obtained from the ESO stellar library is overplotted (the K3 spectral template is taken from Pickles 1998). Given the good agreement, we deem it likely that XRT 140811 is not caused by an extra-galactic FXT but instead by a stellar flare. We manually masked the telluric regions (marked in grey) and a region affected by instrumental artefacts (6030–6100 Å).

by an interloper star (the source adjacent to the host, within $\sim 2\sigma$), and we were unable to extract the spectrum of the candidate host galaxy.

#### *3.2.7 XRT 110621*

The DECam *r*-filter image of the field of XRT 110621 (*bottom* panel of Fig. 1) shows a bright candidate host inside the 1.8 arcsec ($1\sigma$) X-ray position. We adopt the GROND photometry of the candidate host of XRT 110621 from Novara et al. (2020; see Table 3).

We identify the emission lines H$\alpha$ $\lambda$6564.6, H$\beta$ $\lambda$4862.7, H$\gamma$ $\lambda$4341.68, [O III] $\lambda$4960.3, 5008.2, [O II] $\lambda$3727.1, and S II $\lambda$6718.29 in the spectrum of the candidate host galaxy. Our spectroscopic redshift $z_{\rm spec} = 0.0928 \pm 0.0002$ is fully consistent with the redshift determined in Novara et al. (2020).

### 3.3 Fitting the spectral energy distribution

We derived the star formation rate (SFR) and galaxy mass ($M_*$) of the candidate host galaxies using *BAGPIPES* (Bayesian Analysis of Galaxies for Physical Inference and Parameter EStimation; Carnall et al. 2018). Taking into account the star formation history and the transmission function of neutral/ionized ISM for broad-band photometry and spectra, and using the MULTINEST sampling algorithm, BAGPIPES fits stellar population models to the multiband photometric data. Posterior probability distributions for the host galaxy redshift ($z$), age (mass-weighted age; $\rm Age_{MW}$), extinction by dust ($A_V$), specific SFR (sSFR) and metallicity ($Z$) can also be used as free parameters. As priors, we used $A_V$ values between 0.0 and 2.0 mag (flat), an exponentially declining star formation history function, and the parametrization developed by Calzetti et al. (2000) to account for the effect of dust attenuation on the spectral energy distributions (SEDs).

Fig. 7 shows the 16th–84th percentile range for the posterior probability distribution for best-fitting template spectrum and derived broad-band photometry (shaded *grey* and *orange*) for four of the host galaxies. The *blue* points indicate our input photometric data for XRT 030206, XRT 151219, XRT 151128, and XRT 110621. We obtained the posterior probability distribution for the fitted parameters using a flat prior for the redshift given the spectroscopic redshifts and their uncertainties (see Table 6). The posterior probability distribution of the other fitted parameters is shown in the bottom panels of Fig. 7.

## 4 DISCUSSION

We obtained a spectrum of the candidate host of XRT 140811 and found it to be consistent with that of a K star (see Fig. 6). Therefore, we conclude that XRT 140811 might be an K-dwarf flare. Alp & Larsson (2020) also mention XRT 140811 as a possible misidentified Galactic foreground source. Given the source density of objects as bright as or brighter than the candidate host around XRT 140811, there is only a 0.6 per cent chance to find an object close to the FXT position by chance, re-enforcing that the X-ray flare was likely due to a flare on the K star. Stern et al. (2012) shows the dusty torus of an active galactic nucleus (AGN) will typically produce a W1–W2 $\geq 0.8$, where W1 and W2 are Wide-Field Infrared Survey Explorer (WISE) filters at 3.4 and 4.6 $\mu$m, respectively. We calculate the WISE colours W1–W2 $< 0.23$, which suggests that the candidate host is unlikely to be an AGN. To compute the ratio $\log(L_X/L_{\rm bol}) = \log(F_X/F_{\rm bol})$, we normalize stellar synthetic models of dwarf stars (taken from Phillips et al. 2020) to the photometric detections of XRT 140 811 in the $r$ −band, and compute bolometric fluxes by integrating the normalized models at optical/NIR wavelengths. We obtained $\log(F_X/F_{\rm bol}) = -3.42$ for XRT 140811, where $L_X$ and $L_{\rm bol}$ are the X-ray flare and average (non-flare) bolometric luminosities. Dwarf stars typically exhibit ratios not larger than $\log(L_X/L_{\rm bol}) \lesssim -3.0$ (the dwarf star flare saturation limit; e.g. García-Alvarez et al. 2008; De Luca et al. 2020). This check also confirms that XRT 140811 is likely due to a stellar flare.

Therefore, out of the 7 FXTs discussed in this paper and 12 reported by Alp & Larsson (2020), in total, we exclude XRT 140811 as an FXT through our observations, reducing the total FXT count to 11. Among the remaining six FXTs observed by us, we do not have sufficient spectroscopic/photometric information on XRT 160220. We discuss the five other FXTs in detail in the next sections.

We calculated the offset between the centre of the candidate host galaxy and the centre of the FXT localization uncertainty region (see Table 6). If we assume the X-ray uncertainty follows a Gaussian distribution, the distances from the origin for an offset source with Gaussian positional uncertainty follow a Ricean distribution (e.g. Bloom, Kulkarni & Djorgovski 2002). The uncertainty in the offsets are dominated by the uncertainty in the localization of *XMM-Newton* FXTs. Hence, the distribution of the candidate host offsets, considering the $1\sigma$ uncertainty, does not give much information for comparison with the cumulative distribution of galactocentric offset in kpc seen in SGRBs (Fong et al. 2022), LGRBs (Lyman et al. 2017), superluminous supernovae (SL-SNe; Schulze et al. 2021), Type Ia supernovae (Uddin et al. 2020), and core-collapse supernovae (Kelly & Kirshner 2012, Schulze et al. 2021).

Fig. 8 shows the stellar mass and SFR values of the candidate host galaxies compared with host galaxies of other FXT candidates (Quirola-Vásquez et al. 2022), CDFS-XT1(Bauer et al. 2017), CDFS-XT2 (Xue et al. 2019), and XRT 210 423 (Eappachen et al. 2023). The host galaxies of the other transient events, such as LGRBs, SGRBs, and low-luminosity LGRBs [see the references in fig. 13 of Quirola-Vásquez et al. (2022) and Fong et al. (2022)], SN Ia, SN Ib, SN Ic, and SN II, SL-SNe, (Galbany et al. 2014, Schulze et al.

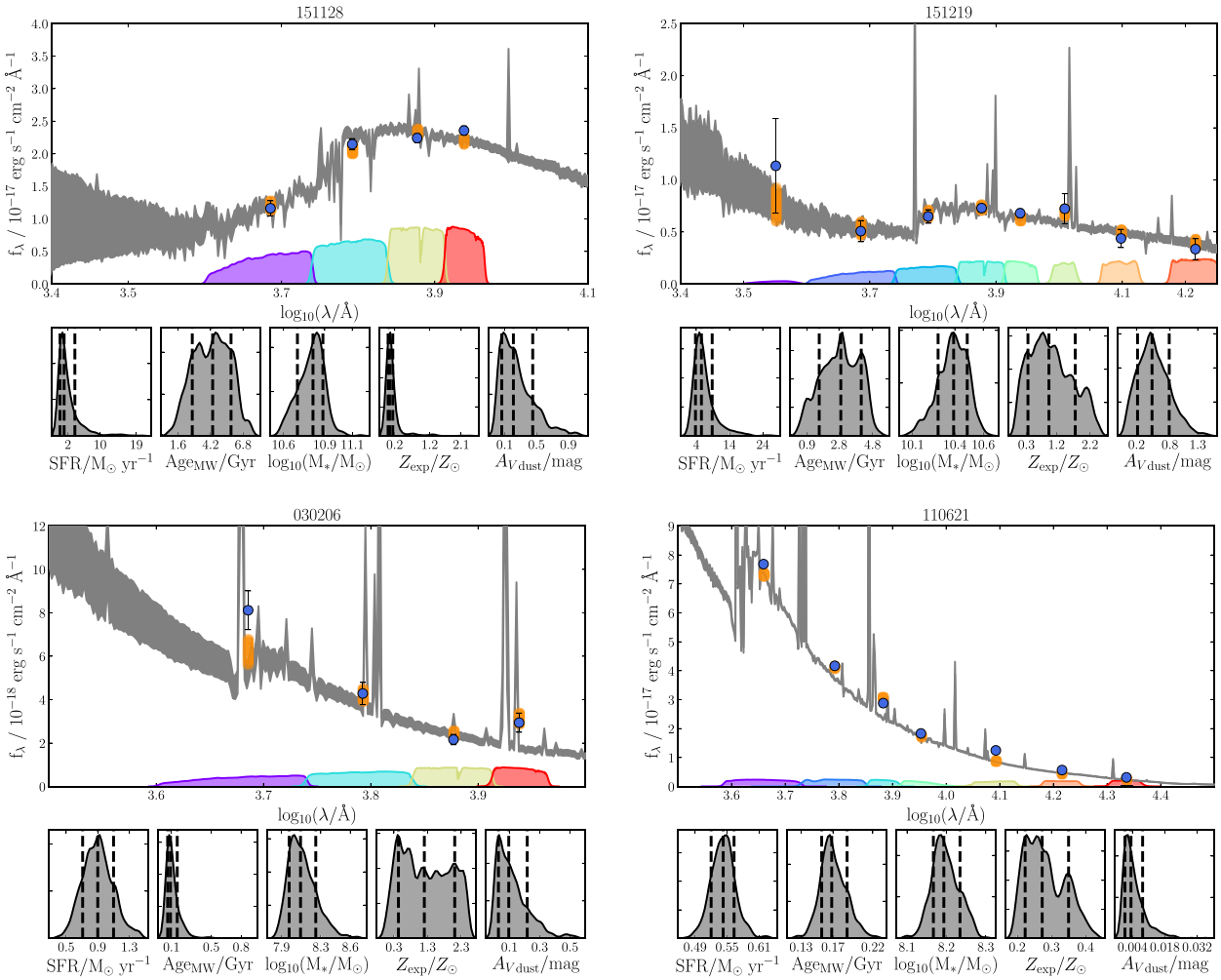


**Figure 7.** Best-fitting SED models obtained using the BAGPIPES package. The 16th–84th percentile range for the posterior probability for the spectrum and photometry (shaded grey and orange, respectively) is shown. The input, observed, photometric data, and their 1$\sigma$ uncertainties are given by the blue markers. The wavelength range covered by the photometric filters is marked by the coloured bars at the bottom of the plot. *Bottom panels:* Posterior probability distributions for the four fitted parameters (SFR, age, galaxy stellar mass, and metallicity). The 16th, 50th, and 84th percentile posterior values are indicated by vertical dashed black lines, from left to right in each sub-plot.

**Table 6.** The inferred host properties of the FXT candidate host galaxies.

| Target | $z_{spec}$ | Angular offset (arcsec) | Physical offset (kpc) | SFR ($M_\odot$ yr$^{-1}$) | Log($M_*[M_\odot]$) | Peak X-ray luminosity of the FXT (erg s$^{-1}$) |
|---|---|---|---|---|---|---|
| XRT 161028⋆ | $0.326 \pm 0.004$ | – | – | – | – | $6 \times 10^{44}$ |
| XRT 161028⋆ | $0.645 \pm 0.0007$ | – | – | – | – | $3 \times 10^{45}$ |
| XRT 030206 | $0.281 \pm 0.003$ | $0.8 \pm 0.8$ | $3.5 \pm 3.5$ | $0.9 \pm 0.3$ | $8.1 \pm 0.2$ | $5 \times 10^{44}$ |
| XRT 151219 | $0.584 \pm 0.009$ | $4.9 \pm 1.3$ | $33.3 \pm 8.9$ | $5.3 \pm 3.4$ | $10.4 \pm 0.1$ | $2 \times 10^{45}$ |
| XRT 151128 | $0.51 \pm 0.01$ | $1.2 \pm 1.8$ | $22.1 \pm 7.6$ | $11.3 \pm 2.6$ | $10.8 \pm 0.1$ | $3 \times 10^{44}$ |
| XRT 110621 | $0.0928 \pm 0.0002$ | $0.6 \pm 1.8$ | $1.1 \pm 3.2$ | $0.54 \pm 0.02$ | $8.19 \pm 0.05$ | $2 \times 10^{43}$ |

We obtain the redshift either from our spectroscopic observations or the photometric redshift through our SED fitting. Host parameters, along with the peak X-ray luminosity of the FXT, assuming it is at the distance of the candidate host, are given. ⋆ We provide two entries for XRT 161028, one for each of the two candidate hosts within the 2$\sigma$ X-ray position (see Section 3.2.1).

2021), TDEs (French et al. 2020), and GW 170817 (Im et al. 2017) are denoted by coloured squares.

The determination of redshift/distance to the hosts of the FXTs allows us to convert the observed FXT (peak) flux to (peak) luminosity. The peak luminosity of the FXT is a powerful tool in distinguishing between the various proposed progenitor models of the FXTs. The progenitor models include BNS mergers ($L_{X,\,peak} \approx 10^{44}$–$10^{51}$ erg s$^{-1}$; Berger 2014), WD-IMBH TDEs ($L_{X,\,peak} \lesssim 10^{48}$ erg s$^{-1}$; Maguire et al. 2020; beamed emission), and SN SBO ($L_{X,\,peak} \lesssim 10^{44}$ erg s$^{-1}$; Soderberg et al. 2008; Waxman

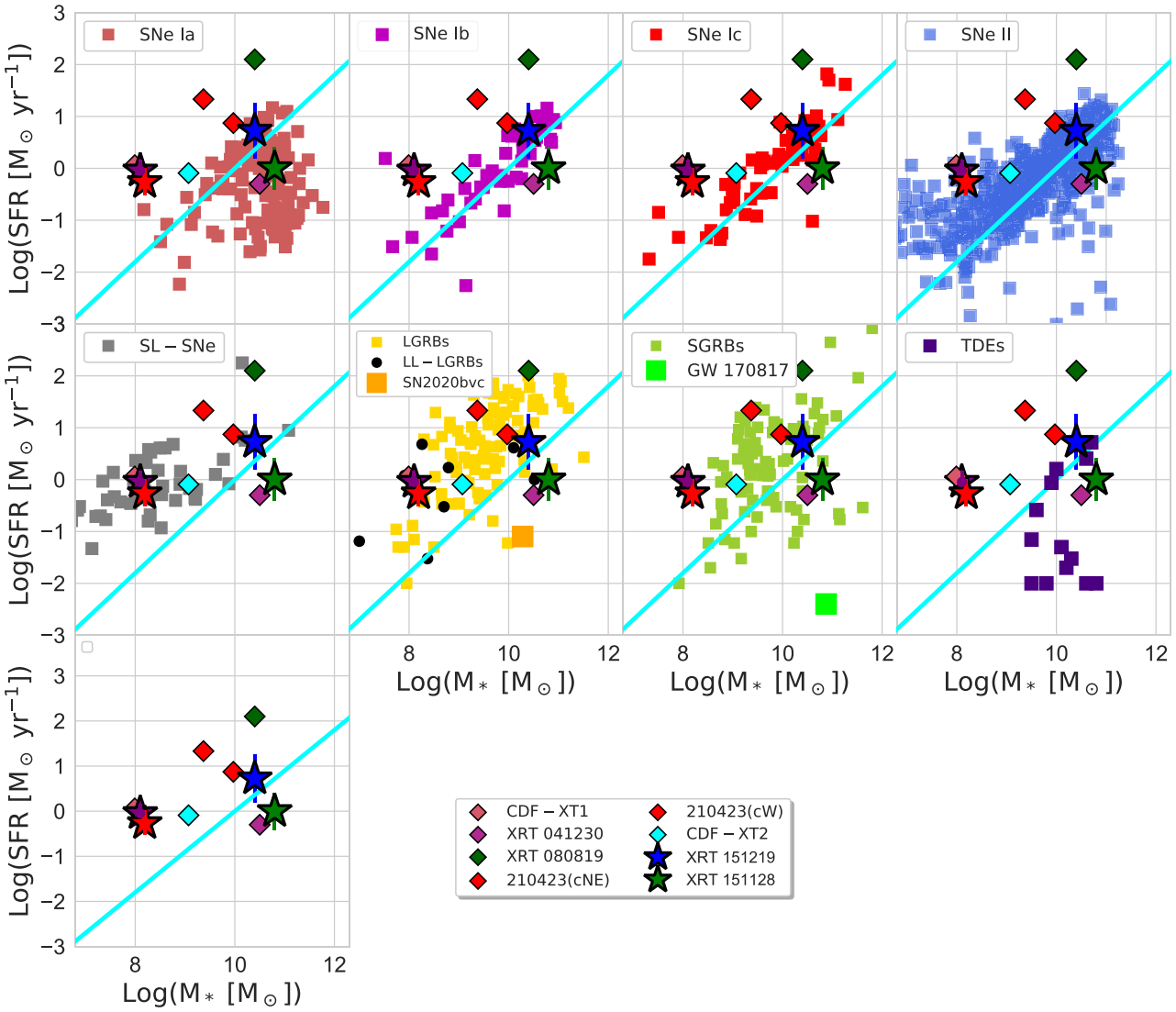


**Figure 8.** $M_*$ and SFR of the candidate host galaxies (coloured stars) compared with host galaxies of other transient events. Different panels show the host properties of the previously reported FXTs (Bauer et al. 2017; Xue et al. 2019; Quirola-Vásquez et al. 2022; Eappachen et al. 2023), of LGRBs, SGRBs, low-luminosity LGRBs [see the references in fig. 13 of Quirola-Vásquez et al. (2022) and Fong et al. (2022)], SN Ia, SN Ib, SN Ic, and SN II (Galbany et al. 2014; Schulze et al. 2021), GW 170817 (Im et al. 2017), and TDEs (French et al. 2020). The solid cyan lines show the best-fittingd local galaxy main sequence relation from Peng et al. (2010).

& Katz 2017; Goldberg, Jiang & Bildsten 2022). We discuss if the *XMM-Newton*-discovered FXTs studied here are due to a SN SBO as suggested by Alp & Larsson (2020). Using our inferred host properties, we also discuss other progenitor models for the FXTs.

For an SN SBO, we expect associated SNe emission to become detectable after some rise time delay. The rise times ($t_r$) for various SNe are as follows: Type II SNe have median rise times of $7.5 \pm 0.3$ d in $g$ (González-Gaitán et al. 2015), whereas Type Ia SNe have a mean rise time of $18.98 \pm 0.54$ d (Firth et al. 2015) and Type Ic SNe have an average $r$-filter rise time of $15 \pm 6$ d (Taddia et al. 2019). Type Ia SNe have a peak absolute magnitude ranging between $-18$ and $-20$ in the $B$-filter, while for Type Ic, it ranges between $-15$ and $-20$ mag in the $B$-filter. For Type II SNe, the distribution of peak absolute magnitude is wider, varying from $-14$ to $-21$ in the $B$-filter (Richardson et al. 2014).

In Fig. 9 we compare our limits on contemporaneous optical counterparts for three of the FXTs, XRT 161028, XRT 151219, and XRT 151128 (see Table 4) with the light curves of GW 170 817 (Cowperthwaite et al. 2017, $g$ and $r$ filters), SN 2008D (Soderberg et al. 2008, $g$, $r$, and $i$ filters), a sample of Type II SNe (Hicken et al. 2017, $V$-filter), a sample of Type Ia SNe (Jha et al. 2006; Matheson et al. 2008, $V$-filter), and the light curves of two Type Ic SNe, SN 2006aj (Modjaz et al. 2006) and SN 1997ef (Iwamoto et al. 2000, both $V$-filter). The comparison samples are first moved into their rest frames before being shifted to the redshift of each FXT. We make no $K$-correction, but note that the difference in rise times resulting from the $K$-correction at these redshifts will not be large. Because the explosion time is unknown for the comparison SNe, the SNe light curves are placed such that the peak occurs at time $t_r$ after the FXT.

The clinching evidence for an FXT and BNS merger association would be the detection of a kilonova signal associated with an FXT.

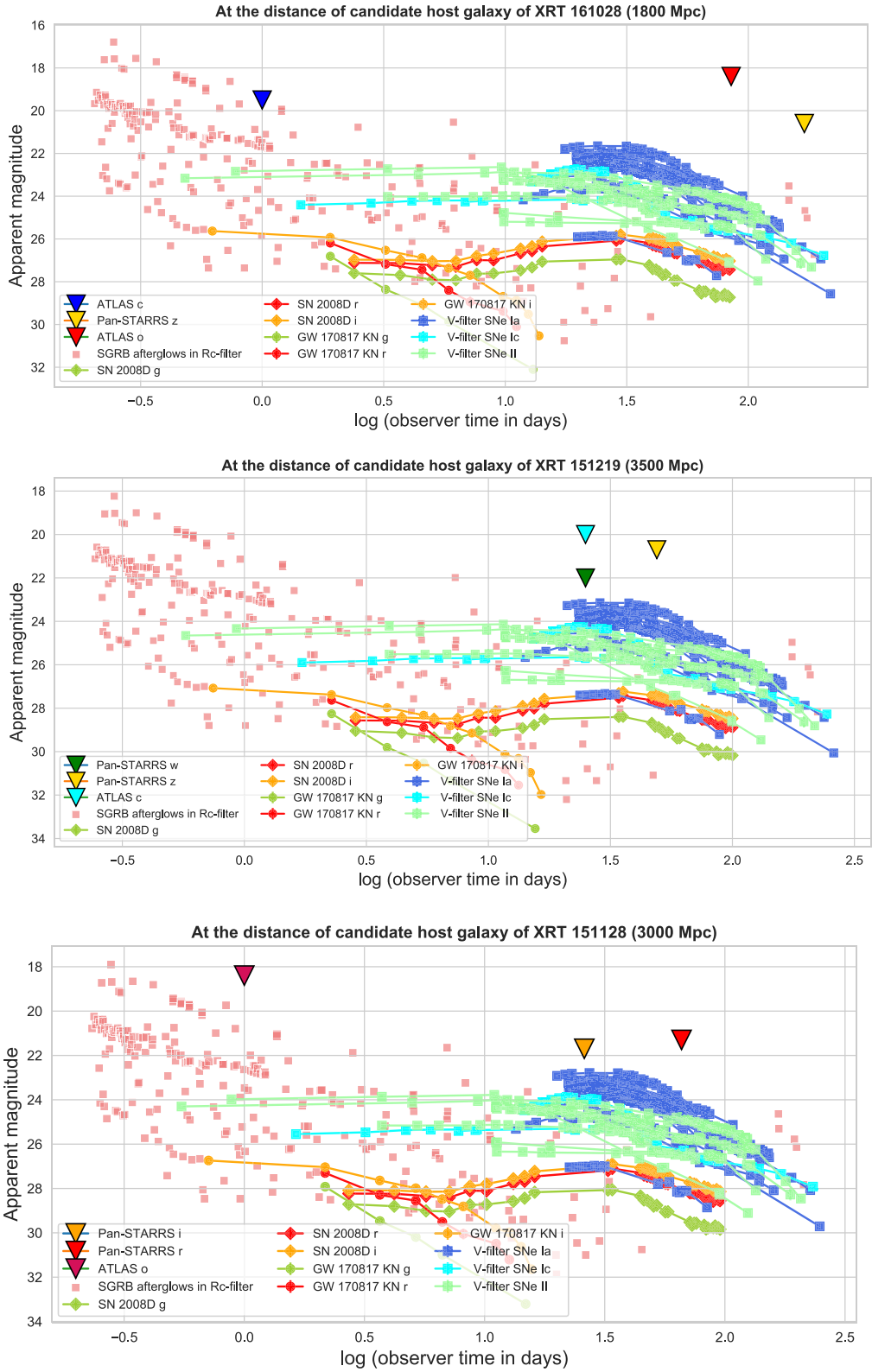


**Figure 9.** We compare our optical limits on contemporaneous optical counterpart emission to three FXTs (shown with coloured triangles) with the light curve of optical signals related to different progenitor models for FXTs. We compare with the light curve of the kilonova associated with GW 170 817 observed in different filters (GW 170 817 KN, g/r/i; Cowperthwaite et al. 2017; shown in circles), with different filter light curves of the supernova associated with the SBO, SN 2008D (Soderberg et al. 2008; diamond symbols), with the light curves of a sample of Type II SNe (Hicken et al. 2017), with a sample of Type Ia SNe (Jha et al. 2006; Matheson et al. 2008), and with the two Type Ic SNe, SN 2006aj (Modjaz et al. 2006) and SN 1997ef (Iwamoto et al. 2000; coloured squares). Observations in different filters are marked using different colours. Unfortunately, our forced photometry results on the detection of a contemporaneous optical counterpart do not rule out any of the optical signals for the progenitor scenarios under discussion in this work.

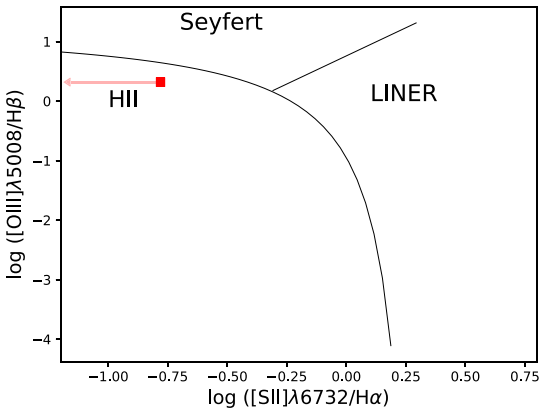


**Figure 10.** BPT diagram (Baldwin, Phillips & Terlevich 1981) using the flux measurements for the emission lines detected in the spectrum of cN. We used the lines H $\alpha$, H $\beta$, [O III], and S II for calculating the position of cN in the BPT diagram. The position of cN falls within the area in the BPT diagram occupied by H II regions. The size of the symbol is larger than the size of the measurement error in the emission line flux ratio log ([O III]/H $\beta$).

Kilonovae are faint, fast-evolving sources powered by radioactive decay from the lanthanides that are formed in the neutron-rich material ejected during the BNS merger (Metzger & Berger 2012). Lanthanide material has very high opacities (Barnes & Kasen 2013); therefore, they emit little in the optical on time-scales beyond a few days and so are expected to be very red sources after a few days. On time-scales of weeks, emission from the atypical Type Ia SN that may accompany the white dwarf disruption is expected to be rather blue with absolute $u$ to $i$-filter magnitudes ranging from $M_U = -16$ to $-19$ and $M_I = -17$ to $-18$ (see fig. 4 in MacLeod et al. 2016). The light curve peaks on a time-scale of ∼1–2 weeks (rest frame).

### 4.1 XRT 161028

We find that the apparent candidate host is a blend of two sources (see Section 3.2.1). The spectroscopic redshift of the first candidate host galaxy (cN) is $z_{\rm spec} = 0.326 \pm 0.004$, which implies a luminosity distance of ∼1300 Mpc considering the cosmology[5] mentioned in the Section 1. If XRT 161028 is associated with this candidate host galaxy, it had a peak luminosity (0.3–10 keV) of $6 \times 10^{44}$ erg s$^{-1}$. This peak X-ray luminosity is too bright for an SN SBO origin. Our second candidate host (cZ) has a redshift $z_{\rm spec} = 0.645 \pm 0.007$. At this redshift, the FXT had a peak X-ray luminosity of $3 \times 10^{45}$ erg s$^{-1}$, firmly ruling out an SN SBO association. There is only a 0.7 per cent chance of finding an object as bright as or brighter than the candidate host so close to XRT 161028 X-ray position by chance. Therefore, we consider it likely that the FXT is associated with either cN or cZ. For cN, using the emission lines H $\alpha$, H $\beta$, [O III] and upper limits on the presence of the S II lines, we calculate the position of the cN in a Baldwin–Phillips–Terlevich (BPT) diagram (Baldwin, Phillips & Terlevich 1981). The position of cN falls within the area in the BPT diagram occupied by H II regions (see Fig. 10; Kewley et al. 2001; Kauffmann et al. 2003; Kewley et al. 2006).

No transient optical light is associated with XRT 161028 in *Pan-STARRS* and ATLAS data to 5$\sigma$ limits. Fig. 9 shows the optical limits obtained from the forced photometry compared with the light curves of GW 170817, SN200D, CC-SNe, Type Ia, and Type Ic SNe, considering the distance of cN (luminosity distance of ∼ 1800 Mpc). We show the magnitude upper limits in ATLAS $c$ (approximately $g + r$-filters), $o$ (approximately $r + i$-filters), and *Pan-STARRS* $z$. If any of these transients was at the redshift of cN, our upper limits are such that our observations would not have yielded in a detection of such a transient. In most cases, we are comparing similar filters. Although the $z$-filter is significantly redder than the comparison filters, even assuming an extremely blue transient (e.g. AT2018cow; Prentice et al. 2018), $r - z$ is only ∼ 0.5. Therefore, the $z$-filter limit is also unconstraining.

### 4.2 XRT 030206

XRT 030206 has a peak X-ray luminosity (0.3–10 keV) of $5 \times 10^{44}$ erg s$^{-1}$ at a redshift of $z_{\rm spec} = 0.281 \pm 0.003$. This is above the peak X-ray luminosity of an SN SBO. The inferred SFR and M$_*$ for the candidate host of XRT 030206 is similar to that of the host population of Type II SNe and SL-SNe.

The candidate host of the FXT XRT 030206 has a chance alignment probability of 0.4 per cent. The peak X-ray luminosity and the inferred SFR and M$_*$ for the candidate host of XRT 030206 suggest that BNS merger origin for this FXT is plausible, while the SN SBO scenario seems unlikely considering the peak X-ray luminosity.

### 4.3 XRT 151219

XRT 151219 is associated with the candidate host galaxy at a redshift of $z_{\rm spec} = 0.584 \pm 0.009$ (luminosity distance of ∼3500 Mpc), it would have a peak X-ray luminosity (0.3–10 keV) of $2 \times 10^{45}$ erg s$^{-1}$. An SBO origin of the XRT 151219 is therefore ruled out (Soderberg et al. 2008; Waxman & Katz 2017; Goldberg, Jiang & Bildsten 2022), but such a peak luminosity is consistent with that predicted for BNS mergers (Berger 2014). The host parameters such as SFR and M$_*$ (blue star in Fig. 8) obtained through the SED fitting for XRT 151219 are consistent with that of a SGRB or SN host.

For XRT 151219, we find no contemporaneous transient counterpart to the 5$\sigma$ limit in the *Pan-STARRS* $w$ (approximately $g + r + i$-filters) and $z$ and ATLAS $c$-filter data. The *middle panel* of Fig. 9 shows the optical limits in comparison with the other transient light curves if they were at the distance of the candidate host galaxy. The upper limits in all the filters are unconstraining.

Given the chance alignment probability of 5.8 per cent, we also consider a scenario where the candidate host galaxy is close to the FXT position by chance. Assuming the distance of the candidate host galaxy at ∼3500 Mpc or further, we derive an upper absolute magnitude limit of $> -19.5$ from the limiting magnitude $m_r = 23.2$ of the *Pan-STARRS* image. If at the distance of the candidate host galaxy, we cannot discard a companion dwarf galaxy host (these absolute magnitudes are similar to that of the Large Magellanic Cloud; Belokurov & Evans 2022). Therefore, we cannot exclude a BNS merger or a WD TDE origin, while the SN SBO is ruled out due to the high peak X-ray luminosity.

However, we find an X-ray flare in *XMM-Newton* serendipitous catalogue within the 3$\sigma$ X-ray region of XRT 151219 centred at (RA, Dec.) = (173.°53113, 0.°87498) with a 1$\sigma$ positional uncertainty of 3.6 arcsec on 2017 June 5. This X-ray flare has a flux of $\sim 4.2 \times 10^{-14}$ erg cm$^{-2}$ s$^{-1}$. Alp & Larsson (2020) also indicates the presence of quiescent emission before and after the XRT 151219 observation. Hence an AGN variability scenario for XRT 151219 also cannot be ruled out.

[5]We use https://www.astro.ucla.edu/wright/CosmoCalc.html

### 4.4 XRT 151128

The spectroscopic redshift of the candidate host galaxy of XRT 151128 is $z_{\rm spec} = 0.509 \pm 0.009$ such that the FXT has a peak X-ray luminosity (0.3–10 keV) of $3 \times 10^{44}$ erg s$^{-1}$, which is slightly above the peak luminosity predicted by the SN SBO models (Waxman & Katz 2017; Goldberg, Jiang & Bildsten 2022). The broad emission lines of the candidate host suggest it is an AGN. The large [O III]/H $\beta$ ratio is also indicative of AGN activity (Baldwin, Phillips & Terlevich 1981). We calculate the WISE colours W1–W2 $= 0.16 \pm 0.14$ and W2–W3 $= 3.54 \pm 0.37$ (W3 band at 12 $\mu$m). There are a variety of reasons why an apparently active galaxy might have inactive mid-infrared colours. Foremost, it is well established that only higher luminosity AGN will have the torus emission dominate over the galaxy stellar emission, causing redder mid-infrared colours (e.g. Moran, Filippenko & Chornock 2002, Eckart et al. 2010). In addition, due to light travel time, a variable AGN that has turned off will not have all of its AGN diagnostic features respond simultaneously (e.g. Saade et al. 2022). Finally, LaMassa et al. (2019) note that different torus dust properties, including an absence of a torus, might explain the failure of WISE colour selection to identify an AGN. The candidate host galaxy occupies the same SFR versus $M_*$ parameter space as most SNe Ia, SNe II host but very few SGRB hosts fall in this region of that parameter space.

We did not detect any counterpart ($5\sigma$) for XRT 151128 in *Pan-STARRS* and ATLAS data to a magnitude limit of 21.7 (*i*-filter) and 21.3 (*r*-filter), 26, and 66 d after the FXT, respectively (see Table 4). We also have an upper limit from ATLAS *o*-filter observations a day after the FXT. However, at the redshift of $z = 0.51$, our upper limits are not deep enough to find a counterpart associated with the FXT XRT 151128 for the models we consider here (see the *bottom* panel of Fig. 9).

We compute the probability of chance alignment of the candidate host galaxy with respect to the X-ray position to be 0.8 per cent. We also consider a scenario where the candidate host is not associated with the FXT. The $5\sigma$ stack limiting magnitudes of *Pan-STARRS* in the *i*-filter is 23.1 mag, which implies a limit of $-19.3$ on the absolute magnitude in the *i*-filter. At this high redshift, we cannot completely discard that there is an unseen dwarf galaxy at the position of the FXT which is the actual host galaxy, as this absolute magnitude limit would still render the Large Magellanic Cloud undetected (Belokurov & Evans 2022). The host properties for XRT 151128 do not allow us to discard the BNS or the WD-IMBH TDE scenario for XRT 151128.

### 4.5 XRT 110621

For XRT 110621 our observations confirm the host candidate properties reported by Alp & Larsson (2020) and Novara et al. (2020). We find that XRT 110621 has a peak (0.3–10 keV) X-ray luminosity of $2 \times 10^{43}$ erg s$^{-1}$ if at the $z_{\rm spec} = 0.0928 \pm 0.0002$ of the candidate host galaxy.

From our SED fitting using *BAGPIPES* to the 7-filter GROND photometry taken from Novara et al. (2020), we derive a SFR and $M_*$ of $0.54 \pm 0.02$ M$_\odot$ yr$^{-1}$ and $\sim 1.5 \times 10^8$ M$_\odot$, respectively, for the host of XRT 110621. These values are similar to those for the hosts of Type II SNe and SL-SNe (see the red star in Fig. 8). The inferred SFR and $M_*$ are similar to the values reported by Novara et al. (2020) who infer an SFR and $M_*$ of $\sim 1$ M$_\odot$ yr$^{-1}$ and $\sim$ (2–3) $\times 10^8$ M$_\odot$ using Galaxy-Observed-Simulated SED Interactive Program and $\sim$ 0.1–1 M$_\odot$ yr$^{-1}$ and $\sim$ (1.5–2) $\times 10^8$ M$_\odot$ using *LePHARE* 'photometric analysis for redshift estimate code' (see Novara et al. 2020). We do not have contemporaneous *Pan-STARRS* photometric data for this FXT. The peak X-ray luminosity is fainter than typically found in SGRBs, furthermore, the candidate host SFR and stellar mass $M_*$ (Fig. 8) instead favours a SN SBO origin. Novara et al. (2020) rules out the possibility of of an possibility of a flare from an AGN for XRT 110621.

## 5 CONCLUSIONS

We present detailed host studies and a contemporaneous optical counterpart search for 7 of the 12 *XMM-Newton* FXTs reported by Alp & Larsson (2020). Of the FXTs discussed in this work, one (XRT 140811) is likely due to a flare from a Galactic late-type star. XRT 110621 is consistent with being due to an SN SBO event. Spectroscopic redshifts for the likely host galaxies for the other four events imply peak X-ray luminosities that are too high to be consistent with SN SBO events. We are unable to discard either the BNS or WD-IMBH TDE scenarios for those four events. For XRT 151219, we also cannot rule out the AGN flare scenario.

## ACKNOWLEDGEMENTS

We thank the anonymous referee for the helpful comments on this manuscript. DE acknowledges discussions with Shubham Srivastava. DMS acknowledges support from the Consejería de Economía, Conocimiento y Empleo del Gobierno de Canarias and the European Regional Development Fund (ERDF) under grant with reference ProID2021010132 (ACCISI/FEDER, UE); as well as support from the Spanish Ministry of Science and Innovation via an Europa Excelencia grant (EUR2021-122010. The work of DS was carried out at the Jet Propulsion Laboratory, California Institute of Technology, under a contract with NASA. We acknowledge support from ANID – Millennium Science Initiative Program – ICN12_009 (FEB, JQ-V), CATA-BASAL – FB210003 (FEB), and FONDECYT Regular – 1190818 (FEB) and 1200495 (FEB). AI and MER acknowledge support by NWO under grant number 184.034.002.

The *Pan-STARRS*1 Surveys (PS1) and the PS1 public science archive have been made possible through contributions by the Institute for Astronomy, the University of Hawaii, the *Pan-STARRS* Project Office, the Max-Planck Society and its participating institutes, the Max Planck Institute for Astronomy, Heidelberg and the Max Planck Institute for Extraterrestrial Physics, Garching, The Johns Hopkins University, Durham University, the University of Edinburgh, the Queen's University Belfast, the Harvard-Smithsonian Center for Astrophysics, the Las Cumbres Observatory Global Telescope Network Incorporated, the National Central University of Taiwan, the Space Telescope Science Institute, the National Aeronautics and Space Administration under Grant No. NNX08AR22G issued through the Planetary Science Division of the NASA Science Mission Directorate, the National Science Foundation Grant No. AST-1238877, the University of Maryland, Eotvos Lorand University (ELTE), the Los Alamos National Laboratory, and the Gordon and Betty Moore Foundation.

This work has made use of data from the Asteroid Terrestrial-impact Last Alert System (ATLAS) project. The Asteroid Terrestrial-impact Last Alert System (ATLAS) project is primarily funded to search for near earth asteroids through NASA grants NN12AR55G, 80NSSC18K0284, and 80NSSC18K1575; byproducts of the NEO search include images and catalogues from the survey area. This work was partially funded by Kepler/K2 grant J1944/80NSSC19K0112 and HST GO-15889, and STFC grants ST/T000198/1 and ST/S006109/1. The ATLAS science products have been made possible through the contributions of the University of Hawaii Institute

for Astronomy, the Queen's University Belfast, the Space Telescope Science Institute, the South African Astronomical Observatory, and The Millennium Institute of Astrophysics (MAS), Chile.

SDSS-IV acknowledges support and resources from the Center for High Performance Computing at the University of Utah. The SDSS website is www.sdss.org. SDSS-IV is managed by the Astrophysical Research Consortium for the Participating Institutions of the SDSS Collaboration including the Brazilian Participation Group, the Carnegie Institution for Science, Carnegie Mellon University, Center for Astrophysics| Harvard & Smithsonian, the Chilean Participation Group, the French Participation Group, Instituto de Astrofísica de Canarias, The Johns Hopkins University, Kavli Institute for the Physics and Mathematics of the Universe (IPMU)/University of Tokyo, the Korean Participation Group, Lawrence Berkeley National Laboratory, Leibniz Institut für Astrophysik Potsdam (AIP), Max-Planck-Institut für Astronomie (MPIA Heidelberg), Max-Planck-Institut für Astrophysik (MPA Garching), Max-Planck-Institut für Extraterrestrische Physik (MPE), National Astronomical Observatories of China, New Mexico State University, New York University, University of Notre Dame, Observatário Nacional/MCTI, The Ohio State University, Pennsylvania State University, Shanghai Astronomical Observatory, United Kingdom Participation Group, Universidad Nacional Autónoma de México, University of Arizona, University of Colorado Boulder, University of Oxford, University of Portsmouth, University of Utah, University of Virginia, University of Washington, University of Wisconsin, Vanderbilt University, and Yale University. This research has made use of the CfA Supernova Archive, which is funded in part by the National Science Foundation through grant AST 0907903.

MAPT acknowledge support from the Agencia Estatal de Investigación del Ministerio de Ciencia e Innovación (MCIN/AEI) and the European Regional Development Fund (ERDF) under grant PID2021-124879NB-I00.

## DATA AVAILABILITY

All data will be made available in a reproduction package uploaded to Zenodo (10.5281/zenodo.10457836).

## REFERENCES

Abdurro'uf et al., 2022, ApJS, 259, 35
Alp D., Larsson J., 2020, ApJ, 896, 39
Baldwin J. A., Phillips M. M., Terlevich R., 1981, PASP, 93, 5
Barnes J., Kasen D., 2013, ApJ, 775, 18
Bauer F. E. et al., 2017, MNRAS, 467, 4841
Belokurov V., Evans N. W., 2022, Nat. Astron., 6, 911
Berger E., 2014, ARA&A, 52, 43
Bertin E., Arnouts S., 1996, A&AS, 117, 393
Bloom J. S., Kulkarni S. R., Djorgovski S. G., 2002, AJ, 123, 1111
Calzetti D., Armus L., Bohlin R. C., Kinney A. L., Koornneef J., Storchi-Bergmann T., 2000, ApJ, 533, 682
Campana S. et al., 2006, Nature, 442, 1008
Carnall A. C., McLure R. J., Dunlop J. S., Davé R., 2018, MNRAS, 480, 4379
Cepa J. et al., 2000, in Iye M., Moorwood A. F.eds, Proc. SPIE Conf. Ser. Vol. 4008, Optical and IR Telescope Instrumentation and Detectors. SPIE, Bellingham. p. 623
Chambers K. C. et al., 2016, preprint (arXiv:1612.05560)
Cowperthwaite P. S. et al., 2017, ApJ, 848, L17
Dai Z. G., Wang X. Y., Wu X. F., Zhang B., 2006, Science, 311, 1127
Dalton G. B. et al., 2006, in McLean I. S., Iye M., eds, Proc. SPIE Conf. Ser. Vol. 6269. SPIE, Bellingham. p. 62690X
Dark Energy Survey Collaboration, 2016, MNRAS, 460, 1270
De Luca A. et al., 2020, A&A, 634, L13
Drlica-Wagner A. et al., 2018, ApJS, 235, 33
Eappachen D. et al., 2022, MNRAS, 514, 302
Eappachen D. et al., 2023, ApJ 948 91
Eckart M. E., McGreer I. D., Stern D., Harrison F. A., Helfand D. J., 2010, ApJ, 708, 584
Edge A., Sutherland W., Kuijken K., Driver S., McMahon R., Eales S., Emerson J. P., 2013, Messenger, 154, 32
Falk S. W., Arnett W. D., 1977, ApJS, 33, 515
Firth R. E. et al., 2015, MNRAS, 446, 3895
Fong W.-f., et al., 2022, ApJ, 940, 56
French K. D., Wevers T., Law-Smith J., Graur O., Zabludoff A. I., 2020, Space Sci. Rev., 216, 32
Galbany L. et al., 2014, A&A, 572, A38
Ganot N. et al., 2016, ApJ, 820, 57
García-Alvarez D., Drake J. J., Kashyap V. L., Lin L., Ball B., 2008, ApJ, 679, 1509
Glennie A., Jonker P. G., Fender R. P., Nagayama T., Pretorius M. L., 2015, MNRAS, 450, 3765
Goldberg J. A., Jiang Y.-F., Bildsten L., 2022, ApJ, 933, 164
González-Gaitán S. et al., 2015, MNRAS, 451, 2212
Greiner J. et al., 2008, PASP, 120, 405
Hicken M. et al., 2017, ApJS, 233, 6
Im M. et al., 2017, ApJ, 849, L16
Irwin J. A. et al., 2016, Nature, 538, 356
Iwamoto K. et al., 2000, ApJ, 534, 660
Jha S. et al., 2006, AJ, 131, 527
Jonker P. G. et al., 2013, ApJ, 779, 14
Kauffmann G. et al., 2003, MNRAS, 346, 1055
Kelly P. L., Kirshner R. P., 2012, ApJ, 759, 107
Kewley L. J., Dopita M. A., Sutherland R. S., Heisler C. A., Trevena J., 2001, ApJ, 556, 121
Kewley L. J., Groves B., Kauffmann G., Heckman T., 2006, MNRAS, 372, 961
Klein R. I., Chevalier R. A., 1978, ApJ, 223, L109
LaMassa S. M., Georgakakis A., Vivek M., Salvato M., Ananna T. T., Urry C. M., MacLeod C., Ross N., 2019, ApJ, 876, 50
Levan A. J. et al., 2014, ApJ, 781, 13
Lin D., Irwin J. A., Berger E., 2021, Astron. Telegram, 14599, 1
Lin D., Irwin J. A., Berger E., Nguyen R., 2022, ApJ, 927, 211
Lyman J. D. et al., 2017, MNRAS, 467, 1795
MacLeod M., Guillochon J., Ramirez-Ruiz E., Kasen D., Rosswog S., 2016, ApJ, 819, 3
McMahon R. G., Banerji M., Gonzalez E., Koposov S. E., Bejar V. J., Lodieu N., Rebolo R., VHS Collaboration, 2013, Messenger, 154, 35
Magnier E. A. et al., 2020, ApJS, 251, 3
Maguire K., Eracleous M., Jonker P. G., MacLeod M., Rosswog S., 2020, Space Sci. Rev., 216, 39
Marsh T., 2019, preprint,(ascl:1907.012)
Massey P., Gronwall C., 1990, ApJ, 358, 344
Matheson T. et al., 2008, AJ, 135, 1598
Matzner C. D., McKee C. F., 1999, ApJ, 510, 379
Metzger B. D., Berger E., 2012, ApJ, 746, 48
Metzger B. D., Piro A. L., 2014, MNRAS, 439, 3916
Metzger B. D., Quataert E., Thompson T. A., 2008, MNRAS, 385, 1455
Modjaz M. et al., 2006, ApJ, 645, L21
Monet D. G. et al., 2003, AJ, 125, 984
Moran E. C., Filippenko A. V., Chornock R., 2002, ApJ, 579, L71
Novara G. et al., 2020, ApJ, 898, 37
Oke J. B. et al., 1995, PASP, 107, 375
Peng Y.-j. et al., 2010, ApJ, 721, 193
Phillips M. W. et al., 2020, A&A, 637, A38
Pickles A. J., 1998, PASP, 110, 863
Planck Collaboration, 2018, A&A, 641, 6
Prentice S. J. et al., 2018, ApJ, 865, L3
Quirola-Vásquez J. et al., 2022, A&A, 663, A168
Quirola-Vásquez J. et al., 2023, A&A, 675, A44
Richardson D., Jenkins R. L. III, Wright J., Maddox L., 2014, AJ, 147, 118

Rosswog S., Ramirez-Ruiz E., Hix W. R., 2009, ApJ, 695, 404
Saade M. L., Brightman M., Stern D., Malkan M. A., García J. A., 2022, ApJ, 936, 162
Saxton R., Komossa S., Auchettl K., Jonker P. G., 2020, Space Sci. Rev., 216, 85
Schawinski K. et al., 2008, Science, 321, 223
Schulze S. et al., 2021, ApJS, 255, 29
Science Software Branch at STScI, 2012, preprint,(ascl:1207.011)
Smith K. W. et al., 2020, PASP, 132, 85002
Soderberg A. M. et al., 2008, Nature, 453, 469
Stern D. et al., 2012, ApJ, 753, 30
Stoppa F., Cator E., Nelemans G., 2023, MNRAS, 524, 1061
Sun H., Zhang B., Gao H., 2017, ApJ, 835, 7
Taddia F. et al., 2019, A&A, 621, A71
Tody D., 1986, in Crawford D. L.ed., Proc. SPIE Conf. Ser. Vol. 627, Instrumentation in Astronomy VI. SPIE, Bellingham. p. 733
Tonry J. L. et al., 2018, PASP, 130, 64505
Uddin S. A. et al., 2020, ApJ, 901, 143
Waxman E., Katz B., 2017, in Alsabti Athem W., Murdin Pauleds., Shock Breakout Theory, Springer-Verlag, Berlin, p. 967
Webb N. A. et al., 2020, A&A, 641, A136
Wilms J. et al., 2020, Astron. Telegram, 13416, 1
Xue Y. Q. et al., 2019, Nature, 568, 198
Zhang B., 2013, ApJ, 763, L22

[1]*SRON, Netherlands Institute for Space Research, Niels Bohrweg 4, 2333 CA, Leiden, the Netherlands*
[2]*Department of Astrophysics/IMAPP, Radboud University Nijmegen, PO Box 9010, 6500 GL, Nijmegen, the Netherlands*
[3]*Instituto de Astrofísica, Pontificia Universidad Católica de Chile, Casilla 306, Santiago 22, Chile*
[4]*Millennium Institute of Astrophysics (MAS), Nuncio Monseñor Sótero Sanz 100, Providencia, Santiago, Chile*
[5]*Observatorio Astronómico de Quito, Escuela Politécnica Nacional, 170136 Quito, Ecuador*
[6]*Instituto de Astrofísica de Canarias, E-38205 La Laguna, S/C de Tenerife, Spain*
[7]*Departamento de Astrofísica, Univ. de La Laguna, E-38206 La Laguna, Tenerife, Spain*
[8]*School of Physics, O'Brien Centre for Science North, University College Dublin, Belfield, Dublin 4, Ireland*
[9]*Space Science Institute, 4750 Walnut Street, Suite 205, Boulder, Colorado 80301, USA*
[10]*Jet Propulsion Laboratory, California Institute of Technology, 4800 Oak Grove Drive, MS 169-224, Pasadena, CA 91109, USA*
[11]*Division of Physics, Mathematics and Astronomy, California Institute of Technology, Pasadena, CA 91125, USA*
[12]*Astrophysics Research Centre, School of Mathematics and Physics, Queen's University Belfast, Belfast BT7 1NN, UK*
[13]*Steward Observatory, University of Arizona, 933 North Cherry Avenue, Tucson, AZ 85721, USA*
[14]*MIT Kavli Institute for Astrophysics and Space Research, 77 Massachusetts Ave., Cambridge, MA 02139, USA*
[15]*Department of Mathematics/IMAPP, Radboud University, PO Box 9010, NL-6500 GL Nijmegen, the Netherlands*
[16]*Cosmic Dawn Center (DAWN), Copenhagen, Denmark*
[17]*Niels Bohr Institute, University of Copenhagen, Jagtvej 128, Copenhagen N 2200, Denmark*
[18]*Racah Institute of Physics, The Hebrew University, Jerusalem 91904, Israel*

This paper has been typeset from a TEX/LATEX file prepared by the author.